Suppression of the Coffee Ring Effect with Undetectable Disturbance of the Deposit

Shiqi Sheng(盛世奇)[1†], Zhening Fang(方浙宁)[2†], Shiyu Gao(高士驭)[1], Ruoyang Chen(陈若阳)[1], Ying Wang(汪颖)[3], Haijun Yang(杨海军)[3*], and Haiping Fang(方海平)[1,4*]

[1]*School of Physics, East China University of Science and Technology, Shanghai 200237, China*
[2]*School of Physical Science and Technology, ShanghaiTech University, Shanghai 201210, China*
[3]*Shanghai Synchrotron Radiation Facility (SSRF), Shanghai Advanced Research Institute, Chinese Academy of Sciences, Shanghai 201204, China*
[4]*Wenzhou Institute, University of Chinese Academy of Sciences, Wenzhou 325001, China*

(Received 30 December 2024; accepted manuscript online 24 January 2025)

Suppressing the coffee ring effect (CRE) of an aqueous suspension through manipulation without affecting the remaining deposit is highly desirable for practical applications; however, this is extremely challenging. Here, we demonstrate CRE suppression with undetectable disturbance of the deposit on carbon-based surfaces. This was achieved by adding ammonium bicarbonate (NH_4HCO_3), which benefits from the dissociation of NH_4HCO_3 to produce NH_4^+, as well as its decomposition into NH_3 and CO_2 molecules. Surprisingly, NH_4^+ can also function as Na^+/K^+ to suppress the CRE through cation interactions, although its hydrate state is only partially positively charged. Moreover, we successfully applied this approach to enhance the morphology, resistance, and color uniformity of deposits of graphene oxide quantum dots, conductive inks, and organic dyes, respectively. This study provides a practical strategy for improving the performance of fabricated devices and paves the way for the development of high-accuracy manufacturing techniques in diverse industries.

DOI: 10.1088/0256-307X/42/2/028101 CSTR: 32039.14.0256-307X.42.2.028101

1. Introduction. The coffee ring effect (CRE), in which a liquid with suspended solutes leaves a ring-shaped deposit as it evaporates on a surface in the constant wetting area mode,[1–3] leads to a non-uniform distribution of the resulting deposits. Although the CRE has been reported to have potential applications in concentrating samples for spectroscopic detections,[4,5] and separating particles within trace samples,[6–8] it has hindered various scientific and industrial applications demanding homogeneous deposits, such as inkjet printing,[9–11] dyeing,[12] micro/nanofabrication,[13–15] diagnostics,[16,17] and electronics.[18–20] Great efforts have been made to suppress the CRE in the past decades, including utilizing organic solvents,[21,22] customizing the suspended particles and/or the substrate,[11,23,24] manipulating the evaporation process with a laser beam,[25] and introducing sol-gel inducers/surfactants/metal salts into the system.[26–33]

Unfortunately, all of these conventional methods have problems in practical applications: organic solvents are unfriendly to both the environment and human beings;[34] the alteration of given suspended particles or substrates is commonly unfavorable for practical use; and laser manipulation requires precise irradiation, which is difficult to control and inconvenient for mass production. Additives that do not change the suspended particles or substrates are commonly used in industry. However, the introduction of surfactants/metal salts has negative effects on the deposit quality, such as reducing the adhesion and contact performance of the deposit due to its adsorption on the surface, or damage to electronic devices due to corrosion of the deposit and the substrate because of the deliquescence of salts. Clearly, a strategy that uses an additive without contaminating the resulting deposit would be ideal. However, the idea of introducing additives into a given suspension without causing them to remain in the deposit seems preposterous.

In this study, we successfully suppressed the CRE while keeping the disturbance to the deposit negligible on carbon-based surfaces, using graphene and polyethylene terephthalate (PET) substrates as examples. This was achieved by adding ammonium bicarbonate (NH_4HCO_3) to the suspension, together with skillful control of the temperature and humidity. We note that carbon-based surfaces pervade natural environments, and their material properties vary; thus, the proposed strategy is expected to be suitable for a wide range of applications. Herein, we applied this strategy to enhance the morphological uniformity of graphene oxide quantum dot (GOQD) deposits, improve the resistance uniformity of poly(3,4-ethylenedioxythiophene) polystyrene sulfonate (PEDOT:PSS) layers, and minimize the chromatic aberration of organic dye patterns. Our analysis shows that

†These authors contributed equally to this work.
*Corresponding author. Email: fanghaiping@sinap.ac.cn; yanghaijun@sinap.ac.cn
© 2025 Chinese Physical Society and IOP Publishing Ltd. All rights, including for text and data mining, AI training, and similar technologies, are reserved.

NH_4HCO_3 produced NH_4^+ to suppress the CRE, and then decomposed into NH_3 and CO_2 molecules, which were removed from the deposit with undetectable disturbance through subtle manipulation. The proposed work introduces a new strategy for realizing improvements in various practical applications, which are usually ignored in conventional research.

2. Materials and Methods.

2.1. Materials. Milli-Q water (Millipore, 18.2 MΩ·cm resistivity) was used for all experiments. Monodisperse polystyrene (PS) and fluorescent polystyrene (F-PS) particle suspensions were purchased from ACME Microspheres, Inc. The following parameters were selected: I) 1.0 μm diameter, 1.00 wt%; II) 0.5 μm diameter, 1.00 wt%; III) 0.2 μm diameter, 1.00 wt%; IV) 1.0 μm diameter, 1.00 wt%, red fluorescent with excitation wavelength λ_{ex} = 535 nm and emission wavelength λ_{em} = 610 nm; and V) 0.2 μm diameter, 1.00 wt%, green fluorescent with excitation wavelength λ_{ex} = 488 nm and emission wavelength λ_{em} = 525 nm. All PS/F-PS particle suspensions were centrifuged, washed, and redispersed in Milli-Q water for five cycles before use. Graphene monolayers on copper foil (300 mm × 245 mm, monolayer coverage > 99%) were manufactured using the chemical vapor deposition (CVD) method by Chongqing Graphene Technology Company. Starch and ammonium hydrogen carbonate (NH_4HCO_3) of analytical grade were provided by Shanghai Aladdin Bio-Chem Technology Co., Ltd. PET films were produced by the Shanghai Zicheng Packaging Materials Company. Acid red 1 was kindly provided by Winchem Industrial Company. A PEDOT:PSS solution with a concentration of 1.30 wt% was provided by Anhui Kuer Bioengineering Co. Ltd. All substrates, salts, and dyes were used as received.

2.2. Synthesis of GOQDs. GOQDs were prepared using a green and effective one-pot hydrothermal method. Starch (0.30 g) was added to 100 mL of Milli-Q water and stirred for 15 min at 60 ℃ with a magnetic stirrer, followed by transference into a Teflon-lined stainless autoclave, which was then heated in an oven at 190 ℃ for 120 min. A pale-yellow suspension was obtained and centrifuged at 15000 rpm for 20 min to remove brown impurities. The concentration of the as-prepared GOQD suspension was approximately 3.0 mg/mL.

2.3. Experimental Setup for Droplet Deposition and Drying. NH_4HCO_3 (1.18 g) was dissolved in Milli-Q water (8.0 mL), followed by adding Milli-Q water to 10.0 mL to prepare an aqueous solution at a concentration of 1.50 M. Then, serial dilution was applied to obtain a series of concentrations.

To prepare the mixture containing monodispersed PS particles, a PS particle suspension (100 μL) with a single particle diameter (1.0, 0.5, or 0.2 μm), Milli-Q water (100 μL), and NH_4HCO_3 solutions (200 μL) with different concentrations were added into Eppendorf tubes and thoroughly mixed with a micropipette (Eppendorf).

Droplets (∼3.0 μL) of the as-prepared mixtures containing PS particles and different concentrations of NH_4HCO_3 were then immediately deposited on the substrate in a petri dish and dried within an environmental control system. The environmental temperature was 20.0 ± 3.5 ℃, and the relative humidity was 70 ± 5%. After evaporation, the deposit together with the substrate was heated for 60 min at 65.0 ℃ to thoroughly remove the NH_4HCO_3. The deposition of GOQD (1.5 mg/mL)/PEDOT:PSS (0.34 wt%)/acid red 1 (5.0 mg/mL) droplets containing different NH_4HCO_3 concentrations was conducted by means of the same procedure.

2.4. Characterization. The reflected bright-field grayscale images of the deposited samples were captured using an optical microscope (Axio Imager, M2m, Zeiss). Images of acid red 1 and PEDOT: PSS deposits were acquired using a digital camera (EOS 80D, Canon) with a macro focus zoom lens. All images were acquired under similar illumination and acquisition settings. These images were displayed without postprocessing. Scanning electron microscopy (SEM) and energy-dispersive X-ray spectroscopy (EDS) images of the PS particle deposition patterns were acquired at room temperature using a scanning electron microscope (LEO 1530VP, Zeiss) operating at 15.0 kV. The resistance of the PEDOT:PSS deposit was measured using a parameter analyzer (4200A-SCS, Keithley) with two probes. The distance between the probe tips was fixed at ∼300 μm during all measurements. The 3D morphologies of the GOQD deposits on the PET substrates were measured using a 3D profilometer (Filmetrics Profilm3D, KLA). Raman spectra were obtained using a Raman microscope (inVia Reflex, Renishaw) operating at 532 nm.

2.5. Grayscale Analysis of the Deposited Patterns. First, we obtained the gray level values of all pixels for each photograph. Then, from the center of the circle, the gray-level values in four directions ($+x$, $-x$, $+y$, $-y$) were determined with respect to the distance from the center. We obtained the average over a 100-pixel width. As the gray-level values increased sharply at the edge region, the values were divided into three regions: the center (Gc), rim (Gr), and substrate (Gs). In the case of acid red 1, the red color channel of the RGB images of the deposit was extracted for the grayscale analysis.

2.6. DFT Calculations. DFT calculations were performed using the Gaussian 09 software.[35–37] B3LYP was chosen as the functional for both the optimization and energy calculations because it is sufficient for describing the leading factors that dominate adsorption. 6-31G* was chosen as the basis set for all atoms. As the carbon-based materials used in the experiments were periodic materials or polymers, it was impossible to simulate the complete molecules with high molecular weights. As an alternative, smaller molecules consisting of fewer periods/monomers were chosen for the simulation, that is, seven aromatic rings for graphene, three monomers for PET, and two monomers for PS (see their molecular configurations in Fig. S1, Supplemental Material). To avoid overestimation of adsorption energy due to oxygen-containing groups, the cluster of water and NH_4HCO_3 was placed near the middle monomer for the PET case. From many initial candidate

geometries, the best structure was determined to possess the lowest total energy, and optimization was performed.

3. Results and Discussion.

3.1. CRE-Suppression of Polystyrene (PS) Suspensions on Graphene Substrate. Suspensions of polystyrene (PS) particles with a diameter of 1.0 μm were thoroughly mixed with NH_4HCO_3 solutions, resulting in PS suspension mixtures with different NH_4HCO_3 concentrations but a constant PS concentration of 0.4 wt%. The mixtures were then separately dripped onto graphene, as shown in Fig. 1(a). The droplets were dried at 20.0 ± 3.5 ℃ with a relative humidity of 70±5% to ensure that the process was extremely slow. At the end of the evaporation process as the deposit was desiccated, the temperature was increased to 65 ℃ and maintained for 60 min to thoroughly remove NH_4HCO_3.

To analyze the uniformity of the deposits, the dried samples were imaged using an optical microscope. Figure 1(b) shows the dried mixture with 60 mM NH_4HCO_3 initially added. The deposit clearly exhibited a uniform

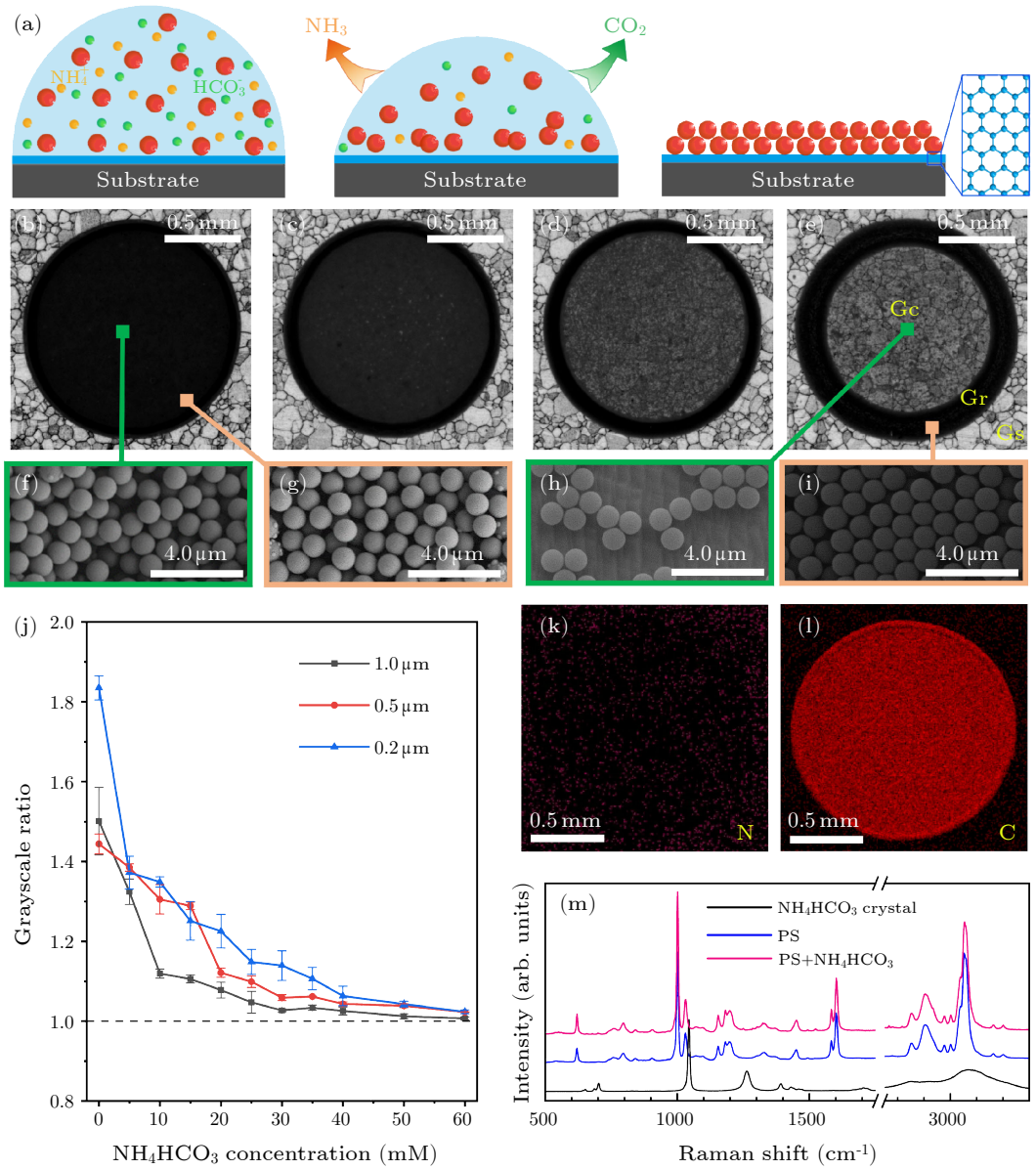

Fig. 1. CRE suppression and NH_4HCO_3 residue analysis for PS particles deposited on a graphene substrate. (a) Schematic of CRE suppression by ammonium cations in a droplet (blue hemisphere) containing PS particles (red beads) with gradual decomposition into ammonia as the droplet evaporates. (b)–(e) Optical microscopy images of droplets containing PS particles (1.0 μm in diameter) mixed with different NH_4HCO_3 concentrations (60, 10, 5, and 0 mM) deposited on graphene. (f)–(i) Magnified images at the center and rim of the corresponding deposition patterns in (b) and (e). (j) GRs [GR = (Gr–Gs)/(Gc–Gs)] of the deposits obtained from PS particles with different diameters on graphene substrates. (k) and (l) SEM–EDS mapping images of N and C within the uniform deposition pattern shown in (b). (m) Raman spectra of PS+NH_4HCO_3 (carmine line), PS (blue line), and NH_4HCO_3 crystal (black line), where PS+NH_4HCO_3 and PS represent the CRE-suppressed pattern deposited from the PS mixture with 60 mM NH_4HCO_3 and the ring-shaped pattern deposited from the PS suspension, respectively.

black pancake character, indicating that the CRE was suppressed. Upon decreasing the NH_4HCO_3 concentration from 10 to 0 mM, the rim and center of the pattern gradually became darker and lighter, respectively [Figs. 1(c)–1(e)]. For the PS suspension without NH_4HCO_3, the deposit displayed a ring-like pattern with a dark rim and a light gray center, which is a typical CRE pattern, as shown in Fig. 1(e). These images show that the introduction of NH_4HCO_3 improved the uniformity of the deposits.

To examine the detailed distribution of the PS particles in the deposits, we next performed SEM analysis. Figures 1(f) and 1(g) show that the densities of the PS particles in the center and at the rim were roughly equal in the sample with the addition of 60 mM NH_4HCO_3. However, when no NH_4HCO_3 was added, most of the PS particles accumulated at the rim, and a considerable amount of space remained in the center where the substrate could be observed [Figs. 1(h) and 1(i)]. All SEM results shown here are consistent with the optical microscopy data.

To quantitatively characterize the uniformity of the deposited PS particles, we computed the grayscale ratio, denoted by $GR = (Gr–Gs)/(Gc–Gs)$, where Gc, Gr, and Gs are the average grayscale values at the pattern center, pattern rim, and substrate, respectively. Here, $GR = 1.0$, which represents $Gc = Gr$, clearly corresponds to a uniform deposit because the grayscale values of the pattern show little difference between the center and the rim. As shown in Fig. 1(j), the GR value for the deposits of the PS mixture with a particle diameter of 1.0 μm sharply decreased and eventually converged to approximately 1.0 as the NH_4HCO_3 concentration increased to 60 mM. Thus, the pattern was essentially uniform at a salt concentration of 60 mM. These results clearly indicate that the CRE can be effectively controlled by the concentration of NH_4HCO_3 in the mixture.

To validate the generality of this strategy, we repeated experiments using PS particles of various sizes (Fig. S2). As shown in Fig. 1(j), the GR values for the deposits of PS mixtures with small particle diameters (i.e., 0.5 and 0.2 μm) also approached 1.0 when 60 mM NH_4HCO_3 was added. Interestingly, the initial GR without NH_4HCO_3 increased as the particle size decreased, indicating that the deposits exhibited a strong CRE for small particles. However, the GR value decreased more quickly with increasing NH_4HCO_3 concentration for small particles, leading to an approximately unchanged NH_4HCO_3 concentration for full suppression. Notably, this strategy is also effective in suppressing the CRE in droplets of mixed solutions containing PS particles of different sizes. As shown in Fig. S3, upon the addition of 60 mM NH_4HCO_3, the deposition formed from a droplet of bi-dispersed fluorescent polystyrene (F-PS) particle solution (containing F-PS particle with diameters of 1.0 and 0.2 μm) exhibited a pancake-like pattern, in which both the 0.2 μm and 1.0 μm PS microspheres were uniformly distributed. These results show that this strategy can be applied to suspended particles of various sizes, although their CREs may be more stubborn.[38] Furthermore, this strategy is effective for a wide range of substrates abundant in aromatic ring structures, such as PET, which is one of the most commonly used polymer materials. As illustrated in Fig. S4, the CRE of PS particles on a PET substrate was completely suppressed by the addition of NH_4HCO_3.

3.2. Undetectable Content of NH_4HCO_3 Remaining. To confirm that no residual NH_4HCO_3 remained after full CRE suppression, we used EDS to analyze the elemental composition of the uniform deposit obtained from the dried PS mixture with 60 mM NH_4HCO_3 initially added. As shown in Fig. 1(k), the nitrogen distribution appeared completely black without any signal of nitrogen, indicating that the NH_4HCO_3 content was negligible, even below the detection limit of EDS (0.1%–0.5%). In contrast, the carbon distribution formed a red pancake pattern, as shown in Fig. 1(l), demonstrating that the carbon from the PS particles was uniformly distributed throughout the deposit. Thus, a major benefit of the strategy developed in this study is that the amount of residual NH_4HCO_3 in the dried deposits is negligible.

The finding that a negligible amount of NH_4HCO_3 remained in the dried deposit was further verified by Raman spectroscopy. As shown in Fig. 1(m), the strong peak at 1050 cm^{-1} in the spectrum of NH_4HCO_3 is ascribed to the asymmetric bending of the NH_4^+ group.[39] However, this peak cannot be observed in the spectrum of the CRE-suppressed deposit for the sample to which 60 mM of NH_4HCO_3 was initially added. Moreover, the Raman spectrum of the CRE-suppressed deposit is almost identical to that of the ring-shaped pattern without NH_4HCO_3 addition. These results also provide strong evidence that the content of NH_4HCO_3 remaining in the dried deposit was extremely low and could not be detected by Raman spectroscopy.

Gas bubbles sometimes formed during evaporation, resulting in holes in the CRE-suppressed deposit and reducing its uniformity. The possibility of gas bubble formation was effectively reduced through careful control of the process, i.e., by initially applying a temperature of approximately 20.0 ± 3.5 ℃ and a relative humidity of approximately 70% to make the evaporation process sufficiently slow until the droplet was dry. Subsequently, the deposit was heated to 65.0 °C and kept at that temperature for 60 min to thoroughly remove NH_4HCO_3 in the deposit. The importance of this control strategy can be more clearly observed in the CRE suppression for GOQDs in the application examples shown below.

3.3. Applications. To demonstrate the potential application of this strategy in a wide range of industries, we evaluated its use in three scenarios. First, we applied this strategy to deposit GOQDs, which exhibit unique electronic, fluorescent, photoluminescent, chemiluminescent, and electro-chemiluminescent properties, making them potentially useful in areas such as sensing, biomedical applications, and optoelectronics.[40] Figures 2(a) and 2(b) show the 3D profiles of the GOQD deposits on PET substrates with and without NH_4HCO_3 added initially. A green color was observed throughout the deposit when the concentration of NH_4HCO_3 was 750 mM, indicating that the thickness was nearly the same. This was further

proven by the flat line in the cross-height profile along the diameter of the CRE-suppressed deposits, shown in Fig. 2(c). In comparison, the profile appeared as a crater when NH_4HCO_3 was absent in the droplet. Therefore, it can be concluded that the crater was filled and the deposit was made uniform with the addition of NH_4HCO_3.

Careful control of the temperature and humidity are crucial throughout the CRE suppression process. Figure 2(d) shows a photograph of the deposit evaporated under careful control of these conditions to decelerate the process; only a few uneven areas were observed. For comparison, Fig. 2(e) shows the image of a deposit intentionally dried quickly through evaporation at ∼25.0 ℃ with a relative humidity of ∼40%, followed by heating for 60 min at 65.0 ℃. Many holes can be clearly observed (Fig. S5), indicating a relatively uneven surface. These results show that by manipulating the evaporation process, the disturbance to the deposits by gas bubbles is further reduced.

Next, we investigated the application of the developed strategy to PEDOT:PSS. PEDOT:PSS is well known as a remarkable conducting polymer with high transparency, favorable mechanical properties and good biocompatibility,[41,42] and uniform resistance throughout the deposit largely improves the accuracy of the devices in which it is used. Photographs of dried PEDOT:PSS on PET substrates, which were obtained using different concentrations of NH_4HCO_3, are shown in Figs. 3(a) and 3(b). Figure 3(a) shows a uniform blue pancake-like image, indicating that the CRE was fully suppressed when the NH_4HCO_3 concentration reached 750 mM.

The resistances of the deposits were then measured using a parameter analyzer (Fig. S6). Both the rim and center had almost the same resistance ($4.23 \pm 0.35 \times 10^8\ \Omega$ and $4.05 \pm 0.17 \times 10^8\ \Omega$, respectively) when 750 mM NH_4HCO_3 was added, as shown in Fig. 3(c). In contrast, a clear CRE was observed [i.e., the rim is much darker than the center in Fig. 3(b)] when NH_4HCO_3 was

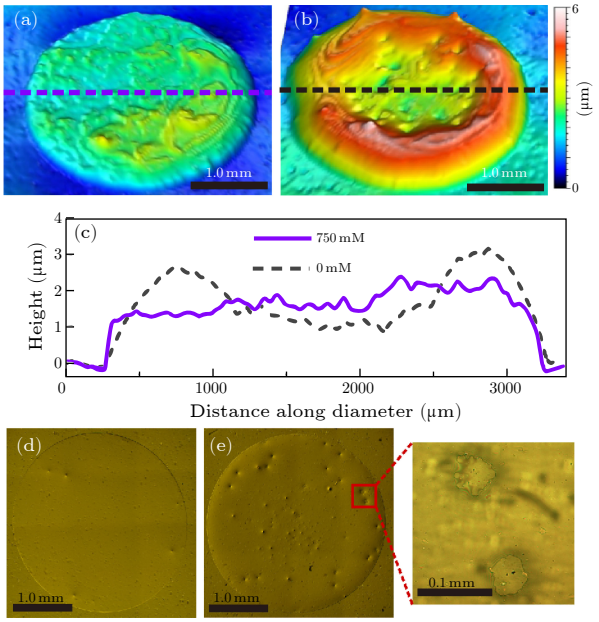

Fig. 2. CRE suppression for GOQDs on a polyethylene terephthalate (PET) substrate. (a)–(c) 3D profiles of patterns deposited from droplets of GOQD mixtures with different NH_4HCO_3 concentrations (750 and 0 mM) on PET films, and corresponding cross-height profiles along the diameter. (d) and (e) Photographs of CRE-suppressed GOQD patterns with/without careful control of the temperature and humidity. The inset in (e) shows a magnified image of the hole.

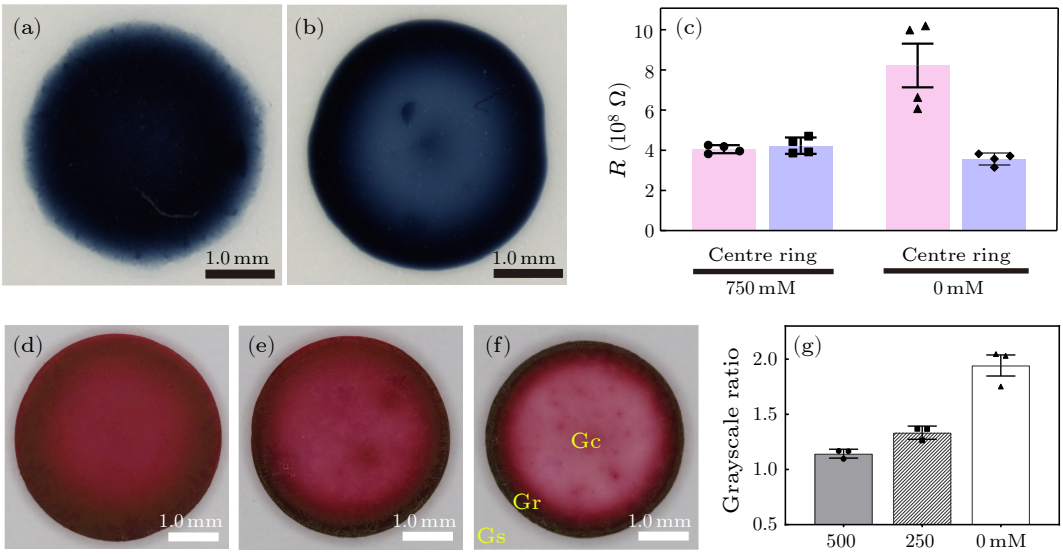

Fig. 3. CRE suppression for PEDOT:PSS and an organic dye. (a) and (b) Photographs of samples deposited from droplets of PEDOT:PSS suspension mixtures with different NH_4HCO_3 concentrations (750 mM and 0 mM) on PET films. (c) Resistance (R) uniformity analysis of the PEDOT:PSS deposits on PET films. (d)–(f) Photographs of samples deposited from droplets of acid red 1 suspension mixtures with different NH_4HCO_3 concentrations (500 mM, 250 mM, and 0 mM) on PET films. (g) GRs of the deposition patterns of acid red 1 on PET films. GR = (Gr–Gs)/(Gc–Gs), where Gc, Gr, and Gs are the average grayscale values at the pattern center, pattern rim, and substrate, respectively.

absent, and the resistance at the center ($8.22\pm1.88\times10^8\,\Omega$) was doubled compared to that at the rim ($3.56\pm0.26\times10^8\,\Omega$). With better uniformity of the deposits, the proposed strategy is expected to facilitate its application in various practical devices, such as solar cells, flexible electronics, and optoelectronic devices.

Finally, we investigated the application of the developed strategy to the organic dye acid red 1, which is widely used in the photo-redox catalysis, textile, leather, paper, and dyeing industries.[43] Clearly, printing performance is improved by achieving a uniform color depth through CRE suppression. Figure 3(d) shows a pancake-like image with a crimson color for the sample obtained by depositing acid red 1 dye on a PET substrate with 500 mM NH_4HCO_3 initially added, suggesting full suppression of the CRE. Similar to the previous results, the contrast between the rim and center increased as the concentration of the introduced NH_4HCO_3 decreased [Fig. 3(e)], and the rim appeared solid black, whereas the center was light red when NH_4HCO_3 was absent [Fig. 3(f)]. We then split the red channel and measured the GR between the rim and center, which increased from ∼1.0 to ∼2.0 as the concentration of NH_4HCO_3 decreased from 500 mM to 0 mM [Fig. 3(g)]. This result indicates that the color throughout the entire pattern was almost completely uniform when an adequate amount of NH_4HCO_3 was added (500 mM), and the printing performance was substantially improved.

3.4. Theoretical Analysis. To understand the underlying physics of CRE suppression with undetectable disturbance of the deposit, we conducted a theoretical analysis. When NH_4HCO_3 is initially added to a droplet, it dissolves in water and dissociates into ions:

$$NH_4HCO_3(s) \xrightarrow{H_2O} NH_4^+(aq) + HCO_3^-(aq). \quad (1)$$

The hydrolyzed cations are attracted to both the suspended particles and the carbon-based substrate via cation–π interactions.[44–46] Consequently, these interactions mediate the adsorption of particles onto the substrate, thereby enhancing the friction between the substrate and particles. This increased friction counteracts the transverse propulsive force that would otherwise carry the particles to the periphery during the evaporation process, thus reducing the CRE, as previously reported.[29]

Density functional theory (DFT) calculations were performed to describe the adsorption behavior between the cations and aromatic molecules. Three different aromatic molecules were chosen as examples for investigation, representing the suspended particles (PS) and substrates (graphene and PET). A cluster consisting of one NH_4^+ cation, one anion, and eight water molecules was placed near the aromatic molecules to simulate the adsorption of NH_4^+ cations in an aquatic environment. As shown in Fig. 4, the NH_4^+ cation dissociated from NH_4HCO_3 tended to adsorb on the aromatic rings through cation–π interactions. The adsorption energies for the 3 systems were determined to be 13.6, 14.6, and 11.5 kcal/mol, denoting that all investigated aromatic molecules were indeed able to attract NH_4^+ cations. Compared to the interaction strength of monovalent metal cations (e.g., ∼25 kcal/mol for Li^+, Na^+, and K^+ on graphene[47]), that of hydrated NH_4^+ cations is much weaker because they are only partially positively charged. However, as the concentration of NH_4HCO_3 increased, more NH_4^+ cations were able to adsorb on the aromatic rings, enhancing the adsorption of the particles on the substrate and leading to the full suppression of the CRE.

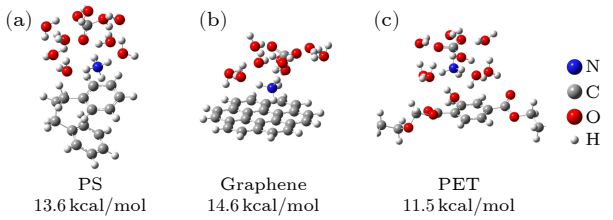

Fig. 4. DFT calculations for the adsorption of a hydrated NH_4^+ cation, dissociated from an NH_4HCO_3 molecule, on aromatic molecules. Optimized structure for NH_4^+ adsorption on (a) PS, (b) Graphene, and (c) PET. The adsorption energy for each system is listed below the picture.

Finally, we considered the process of removing NH_4HCO_3 from the deposit. NH_4HCO_3 can be easily decomposed into carbon dioxide (CO_2), ammonia gas (NH_3), and water,[48] as shown in Eq. (2)

$$NH_4HCO_3 \rightarrow NH_3\uparrow + CO_2\uparrow + H_2O. \quad (2)$$

As water evaporates, NH_4HCO_3 decomposes and leaves the suspension. When the rate of water evaporation is faster than that of the decomposition of NH_4HCO_3, a large amount of NH_4HCO_3 remains in the deposit, and bubbles are produced when NH_4HCO_3 further decomposes. The comparable rates of water evaporation and decomposition of NH_4HCO_3 reduce the quantity of NH_4HCO_3 remaining in the deposit and the occurrence of bubbles. Therefore, careful control of the temperature and humidity was used to reduce the disturbance to the deposit by gas bubbles.

4. Conclusions. We achieved full CRE suppression of aqueous suspensions on carbon-based surfaces with undetectable disturbance to the deposit and substrate by adding ammonium bicarbonate (NH_4HCO_3) and skillfully controlling the temperature and humidity. This strategy is both economical and simple, making it suitable for improving various device fabrications. Surprisingly, NH_4^+ cations dissociated from NH_4HCO_3 can also function as Na^+/K^+ to suppress the CRE through the cation–π interactions although its hydrate state is only partially positively charged. Notably, subtle manipulation of the temperature and humidity can effectively prevent bubble formation due to the NH_3 and CO_2 molecules decomposed from the NH_4HCO_3 molecules, preventing holes in the deposit. The application of this strategy has been demonstrated with GOQDs, PEDOT:PSS, and an organic dye, resulting in a substantial enhancement in morphology, resistance, and color uniformity.

The idea of introducing soluble and decomposable additives to produce ions to suppress the CRE, while removing contamination/impurities by decomposing the additives into gas molecules, is valid not only for NH_4HCO_3;

many similar additives are suitable for different needs in different applications. Thus, this study presents seminal work that will open a new field in CRE suppression with undetectable disturbance to the deposit. Carbon-based surfaces exist widely in nature and demonstrate the inherent ability to attract cations through cation interactions.[45,49–54] Thus, the present work can be extended to a wide range of applications, leading to advances in various industries, particularly those requiring highly uniform and pure deposits, such as injection printing, printed electronics, wearable sensors, solar cells, health diagnosis, and textile dyeing.

Data Availability. The data that support the findings of this study are available within the paper and the Supplemental Material. Additional supporting data generated during the present study are available from the corresponding authors upon reasonable request.

Acknowledgements. We thank Dr. Chen Hou for her help with the SEM experiments. We also acknowledge the support from beamlines 01B, 06B, and 07U, the User Experiment Assist System, and the Big Data Science Center, Shanghai Synchrotron Radiation Facility (SSRF), Shanghai Advanced Research Institute, Chinese Academy of Sciences.

Funding. National Natural Science Foundation of China under Grant No. 12005062 (SS). National Natural Science Foundation of China under Grant No. 11974366 (HF). National Natural Science Foundation of China under Grant No. U1632135 (HY). Fundamental Research Funds for the Central Universities, China (HF).

References

[1] Deegan R D, Bakajin O, Dupont T F, Huber G, Nagel S R, and Witten T A 1997 *Nature* **389** 827
[2] Volcanic cooling underestimated 2014 *Nature* **515** 166
[3] Larson R G 2017 *Nature* **550** 466
[4] Wen J T, Ho C M, and Lillehoj P B 2013 *Langmuir* **29** 8440
[5] Wang W, Yin Y, Tan Z, and Liu J 2014 *Nanoscale* **6** 9588
[6] Trantum J R, Wright D W, and Haselton F R 2011 *Langmuir* **28** 2187
[7] Wong T S, Chen T H, Shen X, and Ho C M 2011 *Anal. Chem.* **83** 1871
[8] Jeong H, Han C, Cho S, Gianchandani Y, and Park J 2018 *ACS Appl. Mater. Interfaces* **10** 22877
[9] Park J U, Hardy M, Kang S J, *et al.* 2007 *Nat. Mater.* **6** 782
[10] Minemawari H, Yamada T, Matsui H, Tsutsumi J y, Haas S, Chiba R, Kumai R, and Hasegawa T 2011 *Nature* **475** 364
[11] Mampallil D and Eral H B 2018 *Adv. Colloid Interface Sci.* **252** 38
[12] Bian X, Fan S, Xia G, Chae Y, Yu H, and Xin J H 2022 *J. Cleaner Prod.* **379** 134853
[13] Fan H Y, Lu Y F, Stump A, Reed S T, Baer T, Schunk R, Perez-Luna V, López G P, and Brinker C J 2000 *Nature* **405** 56
[14] Li X, Tian J, Garnier G, and Shen W 2010 *Colloids Surf. B* **76** 564
[15] Han W and Lin Z 2012 *Angew. Chem. Int. Ed.* **51** 1534
[16] Devineau S, Anyfantakis M, Marichal L, Kiger L, Morel M, Rudiuk S, and Baigl D 2016 *J. Am. Chem. Soc.* **138** 11623
[17] Sefiane K, Duursma G, and Arif A 2021 *Adv. Colloid Interface Sci.* **298** 102546
[18] Diao Y, Tee B C K, Giri G, Xu J, Kim D H, Becerril H A, Stoltenberg R M, Lee T H, Xue G, Mannsfeld S C B, and Bao Z 2013 *Nat. Mater.* **12** 665
[19] Zhang D, Peng L, Shang X, Zheng W, You H, Xu T, Ma B, Ren B, and Fang J 2020 *Nat. Commun.* **11** 2603
[20] Fan B, Xiong J, Zhang Y, Gong C, Li F, Meng X, Hu X, Yuan Z, Wang F, and Chen Y 2022 *Adv. Mater.* **34** 2201840
[21] Hu H and Larson R G 2006 *J. Phys. Chem. B* **110** 7090
[22] Pahlavan A A, Yang L S, Bain C D, and Stone H A 2021 *Phys. Rev. Lett.* **127** 024501
[23] Yunker P J, Still T, Lohr M A, and Yodh A G 2011 *Nature* **476** 308
[24] He A, Yang H, Xue W, Sun K, and Cao Y 2017 *Opt. Lett.* **42** 3936
[25] Ta V D, Carter R M, Esenturk E, Connaughton C, Wasley T J, Li J, Kay R W, Stringer J, Smith P J, and Shephard J D 2016 *Soft Matter* **12** 4530
[26] Sempels W, De Dier R, Mizuno H, Hofkens J, and Vermant J 2013 *Nat. Commun.* **4** 1757
[27] Erbil H Y 2015 *Adv. Colloid Interface Sci.* **222** 275
[28] Liu X, Sheng S, Yang H, He Z, Yang Y, Sheng N, Fang H, and Shi G 2020 *ACS Appl. Mater. Interfaces* **12** 38638
[29] Yang H, Yang Y, Sheng S, Wen B, Sheng N, Liu X, Wan R, Yan L, Hou Z, Lei X, Shi G, and Fang H 2020 *Chin. Phys. Lett.* **37** 028103
[30] Sheng S, Fang Z, Yang H, and Fang H 2023 *J. Phys. Chem. B* **127** 10615
[31] Gustavsson K, Jucha J, Naso A, Lévêque E, Pumir A, and Mehlig B 2017 *Phys. Rev. Lett.* **119** 254501
[32] Li L, Huang Z, Meng X, Xing Z, Fan B, Li J, and Chen Y 2024 *Adv. Mater.* **36** 2310752
[33] Howard N S, Archer A J, Sibley D N, Southee D J, and Wijayantha K G U 2023 *Langmuir* **39** 929
[34] Wagare D S, Shirsath S E, Shaikh M, and Netankar P 2021 *Environ. Chem. Lett.* **19** 3263
[35] Frisch M J, *et al. Gaussian 09, Revision A.02*, Gaussian Inc., Wallingford CT, 2009.
[36] Burke K and Wagner L O 2013 *Int. J. Quantum Chem.* **113** 96
[37] Gillan M J, Alfè D, and Michaelides A 2016 *J. Chem. Phys.* **144** 130901
[38] Sheng S, Yang H, Song Y, Chen R, Liang S, and Fang H 2022 *Int. J. Mol. Sci.* **23** 8055
[39] Zhou H, Wang F, Xu M, Liu B, Liu F, Zhang L, Xu X, Sun X, and Wang Z 2016 *J. Cryst. Growth* **450** 6
[40] Li M, Chen T, Gooding J J, and Liu J 2019 *ACS Sens.* **4** 1732
[41] Shi H, Liu C, Jiang Q, and Xu J 2015 *Adv. Electron. Mater.* **1** 1500017
[42] Ray T R, Choi J, Bandodkar A J, Krishnan S, Gutruf P, Tian L, Ghaffari R, and Rogers J A 2019 *Chem. Rev.* **119** 5461
[43] Nicewicz D A and Nguyen T M 2014 *ACS Catal.* **4** 355
[44] Jiang J, Mu L, Qiang Y, Yang Y, Wang Z, Yi R, Qiu Y, Chen L, Yan L, and Fang H 2021 *Chin. Phys. Lett.* **38** 116802
[45] Mahadevi A S and Sastry G N 2013 *Chem. Rev.* **113** 2100
[46] Zhang Z J, Yang Y Z, Jiang J, Chen L, Liang S S, and Fang H P 2022 *Chin. Phys. Lett.* **39** 108201
[47] Mu L, Yang Y, Liu J, Du W, Chen J, Shi G, and Fang H 2021 *Phys. Chem. Chem. Phys.* **23** 14662
[48] Tiefenbacher K F 2017 *The Technology of Wafers and Waffles I. Operational Aspects* (Academic Press) p. 227
[49] Ma J C and Dougherty D A 1997 *Chem. Rev.* **97** 1303
[50] Nair R R, Wu H A, Jayaram P N, Grigorieva I V, and Geim A K 2012 *Science* **335** 442

[51] Chen L, Shi G, Shen J, Peng B, Zhang B, Wang Y, Bian F, Wang J, Li D, Qian Z, Xu G, Liu G, Zeng J, Zhang L, Yang Y, Zhou G, Wu M, Jin W, Li J, and Fang H 2017 *Nature* **550** 380

[52] Zhang L, Shi G, Peng B, Gao P, Chen L, Zhong N, Mu L, Zhang L, Zhang P, Gou L, Zhao Y, Liang S, Jiang J, Zhang Z, Ren H, Lei X, Yi R, Qiu Y, Zhang Y, Liu X, Wu M, Yan L, Duan C, Zhang S, and Fang H 2020 *Natl. Sci. Rev.* **8** nwaa274

[53] Zhao G and Zhu H 2020 *Adv. Mater.* **32** 1905756

[54] Xia X M, Zhou F, Xu J, Wang Z T, Lan J, Fan Y, Wang Z K, Liu W, Chen J L, Feng S S, Tu Y S, Yang Y Z, Chen L, and Fang H P 2022 *Nat. Commun.* **13** 7247